Biophysical Journal Volume 69 October 1995 1230–1245

Incorporation of Surface Tension into Molecular Dynamics Simulation of an Interface: A Fluid Phase Lipid Bilayer Membrane

S.-W. Chiu,* M. Clark,‡ V. Balaji,* S. Subramaniam,*§ H. L. Scott,‡ and E. Jakobsson*§

*National Center for Supercomputing Applications, University of Illinois, Urbana, Illinois 61801; ‡Department of Physics, Oklahoma State University, Stillwater, Oklahoma 74078; and §Department of Physiology, §Center for Biophysics and Computational Biology, and §Beckman Institute for Advanced Science and Technology, University of Illinois, Urbana, Illinois 61801 USA

ABSTRACT In this paper we report on the molecular dynamics simulation of a fluid phase hydrated dimyristoylphosphatidylcholine bilayer. The initial configuration of the lipid was the x-ray crystal structure. A distinctive feature of this simulation is that, upon heating the system, the fluid phase emerged from parameters, initial conditions, and boundary conditions determined independently of the collective properties of the fluid phase. The initial conditions did not include chain disorder characteristic of the fluid phase. The partial charges on the lipids were determined by ab initio self-consistent field calculations and required no adjustment to produce a fluid phase. The boundary conditions were constant pressure and temperature. Thus the membrane was not explicitly required to assume an area/phospholipid molecule thought to be characteristic of the fluid phase, as is the case in constant volume simulations. Normal to the membrane plane, the pressure was 1 atmosphere, corresponding to the normal laboratory situation. Parallel to the membrane plane a negative pressure of −100 atmospheres was applied, derived from the measured surface tension of a monolayer at an air-water interface. The measured features of the computed membrane are generally in close agreement with experiment. Our results confirm the concept that, for appropriately matched temperature and surface pressure, a monolayer is a close approximation to one-half of a bilayer. Our results suggest that the surface area per phospholipid molecule for fluid phosphatidylcholine bilayer membranes is smaller than has generally been assumed in computational studies at constant volume. Our results confirm that the basis of the measured dipole potential is primarily water orientations and also suggest the presence of potential barriers for the movement of positive charges across the water-headgroup interfacial region of the phospholipid.

INTRODUCTION

Modeling a pure phospholipid bilayer is an important step toward modeling the entire environment for a large class of biomolecular processes, i.e., those that take place within biological membranes. Membrane modeling poses a set of technical problems and scientific issues that have not yet been resolved. For instance, membranes in their biological state are disordered liquid crystals of essentially infinite extent. Any truncation of the system cuts off the possibility of observing, for example, bending and splay motions of the system having characteristic wavelengths that are comparable to or greater than the size of the simulated system. The membrane environment is anisotropic, with both the compressibility of the membrane and the effective pressure differing in the dimension normal to the membrane plane as compared with the dimensions in the membrane plane. Whereas the pressure normal to the membrane plane is that of the laboratory, for example, 1 atmosphere, the effective pressure parallel to the membrane plane at the water-lipid interface must be negative, based on measurements of surface tension (Israelachvili et al., 1980).

The precise structure of the membrane is labile and constantly changing. Nuclear magnetic resonance (NMR) studies have given us data on the mean orientations of hydrocarbon tails (Borle and Seelig, 1983; Rice and Oldfield, 1979; McCabe et al., 1994). NMR and neutron and x-ray diffraction have given us data on the mean orientations of the headgroups (Wiener and White, 1992b; Sanders, 1993). But one expects the fluctuations about the mean to be enormous, because liquid crystal theory tells us that large deformations of the membrane can be accomplished with thermal energy at physiological temperatures (Helfrich and Jakobsson, 1990). Indeed, direct evidence from neutron and x-ray diffraction studies tells us that the distribution of positions along the normal to the membrane plane of particular phospholipid atoms is as much as 15 Å wide (Wiener and White, 1992b). Thus the surface of the membrane is very rough. NMR studies suggest that 11–16 water molecules per phospholipid molecule are associated with the membrane, which probably means that they are interdigitating with the polar headgroups in the interfacial region. (Borle and Seelig, 1983). There is also an enormous electric field in the interfacial region. Measurements from several laboratories show that there is an electric potential difference of several hundred millivolts between the hydrocarbon interior of the membrane and the electrolyte (Flewelling and Hubbell, 1986).

Because biological membranes are generally found in liquid crystalline phases, meaningful and useful atomic level models must be dynamic rather than static. It is possible to put phospholipids into crystalline solids (Hauser et al., 1981), but the biological state of membranes is far

Received for publication 12 January 1995 and in final form 30 June 1995.

Address reprint requests to Dr. Eric Jakobsson, NCSA, 4039 Beckman Institute, University of Illinois, 405 N. Mathews, Urbana, IL 61801. Tel.: 217-244-2896; Fax: 217-244-2909; E-mail: jake@ncsa.uiuc.edu.

0006-3495/95/10/1230/16 $2.00

from this solid crystalline state. Thus molecular dynamics, Monte Carlo, or stochastic dynamics methods are necessary to describe biological membranes at an atomic level of resolution. This paper will focus on molecular dynamics simulations of membranes. The choice of the model system, i.e., number of lipid and solvent molecules, choice of boundary conditions, nature of interaction potentials, and the method for equilibration bear significantly on the validity of computation. We will address these issues with a view to elucidating the reasons for the choices we made in our simulations.

Computations of membrane patches have been reported with stochastic boundary conditions (Heller et al., 1993; Zhou and Schulten, 1995), with periodic boundary conditions at constant volume (Venable et al., 1993; Alper et al., 1993a,b; Damodaran and Merz, 1994, Robinson et al., 1994), and with periodic boundary conditions at constant pressure (Egberts, 1988; Berendsen et al., 1992; Chiu et al., 1992; Marrink et al., 1993; Egberts et al., 1994; Huang et al., 1994). Each choice is fraught with trade-offs. The appropriate choice may depend on the experimental conditions under consideration.

Stochastic boundary conditions may inhibit chain tilting of the boundary lipid, which will in turn affect tilting in the rest of the simulation cell. In addition, they fail to simulate the essentially infinite bilayer system. However, they have the advantage that, with a finite delimited computational space, it is feasible to eliminate cutoffs of electrostatic forces within the computational space by use of a multipole method (Board et al., 1992), but it is not clear that electrostatic forces longer than a reasonable cutoff distance, 15 Å or so, are a significant modulator of membrane dynamics and structure. However, it probably is important to use neutral group-based rather than atom-based cutoffs. Atom-based cutoffs are likely to introduce spurious polarizations, based on single atoms of a group being on different sides of a cutoff distance. In using group-based cutoffs, each water and phospholipid molecule may be treated as a group (Damodaran and Merz, 1994). However, it is more economical in nonbonded interactions to divide the phospholipid molecule into several charge groups. When simulating neutral lipids, it is appropriate for the submolecular charge groups to be neutral. This can generally be done with only minor adjustments to the computed partial charges, well within their inherent range of uncertainty. If it is deemed desirable to eliminate cutoffs altogether, a possible reasonably efficient technique to eliminate cutoffs in simulations with periodic boundary conditions is the particle mesh method for Ewald sums (Darden et al., 1993).

Periodic boundary conditions are natural for the membrane system, because they naturally emulate the membrane's effectively infinite extent. A concern, however, is that periodic boundary conditions may introduce spurious collective motions or orientations, for example, an excessive collective tilt of the hydrocarbon chains. This effect might be mitigated by making the box size large enough that the boundaries would have little effect on the interior of the box, but of course this is at the cost of less economical computation. If periodic boundary conditions are to be used at constant volume, it is necessary to be confident of the density of material in the lipid and at the lipid-electrolyte interface. This is possible in a multi-lamellar preparation of known water content, such as the dioleoylphosphatidylcholine membrane that is the subject of a series of papers from the laboratory of White (Wiener and White, 1992a,b). In this case, constant volume calculations would seem justified. However, in simulating a situation where there is excess water, an alternative is to do the computations at constant pressure. In this method, pressure components in each spatial dimension are calculated according to a virial expression, and the dimensions of the box are adjusted slowly during the simulation until the mean internal virial matches the external applied pressure, which is set as a boundary condition (Berendsen et al., 1984). This method, with the external pressure at 1 atmosphere, has been used by the laboratory of Berendsen (Berendsen et al., 1992) and by us (Chiu et al., 1992). In this paper we report on a variant of this method in which the lateral pressure (in the plane of the membrane), rather than being set to the external laboratory pressure of 1 atmosphere, is set according to the measured surface tension at the membrane-water interface. This surface tension can be derived from the pressure-density curve of a monolayer in a Langmuir trough and the surface tension for a pure air-water interface. The derivation we used will be given in Methods.

The force fields for the lipid and water molecules are also a matter of some concern. In a previous constant pressure simulation at 1 atmosphere, it was found that the partial charges in the lipid molecules had to be reduced to produce a fluid phase in a simulated dipalmitoylphosphatidylcholine (DPPC) membrane (Berendsen et al., 1992). In this paper we will explore whether the anisotropic constant pressure boundary conditions described above can produce an appropriate fluid phase in a simulated phosphatidylcholine (PC) membrane with full charges on the lipid molecules. The validity of the simulations will be judged by correspondence to a variety of experimental observations.

METHODS

The simulations were done with the GROMOS (Hermans et al., 1984; van Gunsteren and Berendsen, 1987) molecular simulation suite of programs, with some modifications that are included in the description of methods below.

The simulation system contained 100 dimyristoylphosphatidylcholine (DMPC) molecules, a bilayer with 50 lipid molecules in each monolayer. The initial conformation was the x-ray crystal structure (Hauser et al., 1981). The structure was solvated by 2100 water molecules at a distance of 2.3 Å, providing for a total of 10,990 atoms in the simulation. The initial conformation of the system is shown in Fig. 1 *A*.

The extended simple point charge (SPC/E) water model was used (Berendsen et al., 1987). The SPC/E water model gives more realistic values of both the self-diffusion coefficient and the dielectric constant than does the SPC model. The improved dielectric constant should give better screening of the charges on the polar groups of the phospholipids than does the SPC model. (Inadequate screening of those charges has been cited as a problem in previous lipid bilayer computations (Berendsen et al., 1992)).

The partial charges on the phospholipids were calculated by ab initio electronic structure computations with the GAUSSIAN 92 program at

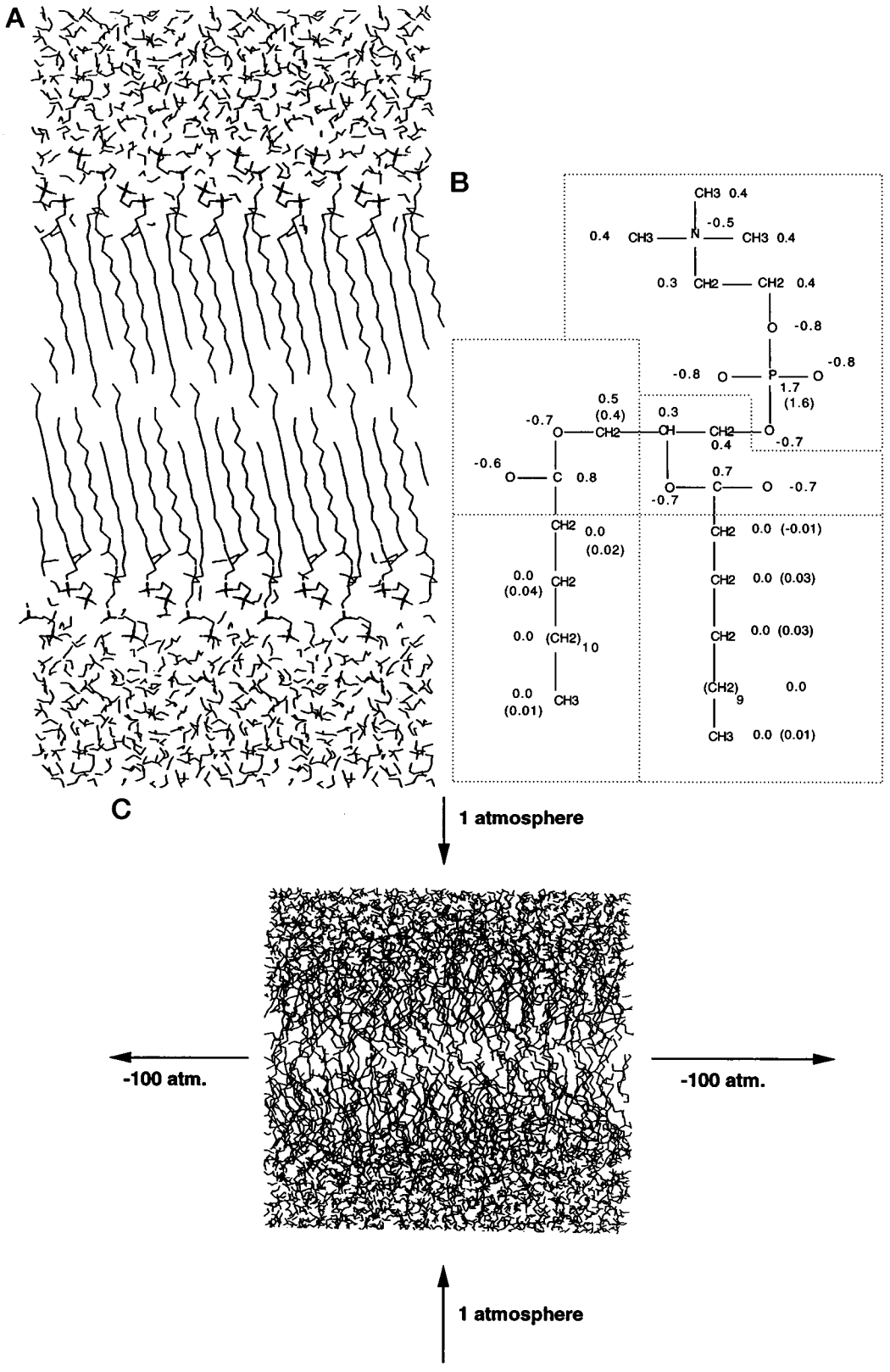

FIGURE 1 (*A*) Initial conformation of the computed system, in the x-ray crystal structure with water added to each side of the bilayer. (*B*) Charge distribution and charge groups used in the simulations. The numbers next to each charged atom are the partial charges, in units of an electronic charge, used in the simulation. The numbers in parentheses are the partial charges actually computed by the Gaussian computations. The difference is an adjustment to be able to divide the phospholipid into neutral charge groups. The charge groups are delineated by dotted outlines. (*C*) The constant pressure boundary conditions used in the simulations. The negative lateral pressure corresponds to the surface tension at the hydrocarbon-water interface. Boundary conditions were periodic in all three dimensions.

Hartree-Fock self-consistent field (SCF) level with the 6–31G* basis set. The partial atomic charges were extracted from the SCF total electron density by Mulliken (1955) population analysis. Fig. 1 *B* shows the partial atomic charges as computed and as used in the simulations. The calculated charges were modified slightly for use in the simulations, so that each phospholipid molecule could be divided into several neutral charge groups for purposes of the electrostatics calculations. The neutral groups are delineated in Fig. 1 *B*. Aside from the partial charges, the phospholipid parameters used were those of Egberts (1988), including the use of the Ryckaert-Bellemans (1975, 1978) potential for the hydrocarbon torsion angles. The extended atom model was used for all nonpolar hydrogens; only polar hydrogens were included explicitly.

The nonbonded interactions were group based. The cutoff distance for calculating nonbonded interactions was 20 Å. A double cutoff was used. For groups within 10 Å of each other the nonbonded interactions were calculated every time step. From 10 to 20 Å the nonbonded interactions were calculated every 10 time steps. At <10 Å both van der Waals and electrostatic interactions were calculated. Between 10 and 20 Å only electrostatic interactions were calculated. The nonbonded interaction pair lists were updated every 25 time steps. No switching function was used. The time step was 2 fs.

Periodic boundary conditions were applied in all three dimensions. The boundary conditions for the simulation were constant pressure, but differ from previous applications in that the pressure was anisotropic. The pressure boundary conditions are shown schematically in Fig. 1 *C*. In the direction normal to the plane of the membrane the pressure is that of the laboratory, typically 1 atmosphere. Within the plane of the membrane the pressure is effectively negative, because of the surface tension at the water-lipid interface.

The following logic was used to estimate the magnitude of the appropriate negative pressure for the simulations. We looked at published data for the experimental relationships among temperature, area, and interfacial pressure for a PC monolayer at an air-water interface. The advantage of the monolayer is that the interfacial pressure can be set by the experimenter. A rather complete set of data is given in Albrecht et al., 1978. The curve of either temperature or pressure versus area shows an abrupt change in slope that corresponds to a phase change. We now look for the value of the interfacial pressure at which the phase change occurs at the same temperature as does the phase change for a bilayer. We reason that this is a good approximation to one-half of the interfacial pressure in a bilayer of a PC membrane. From the data of Albrecht et al. (1978), a value of the interfacial pressure that gives a phase change for DPPC at approximately the same temperature (314 K) as the bilayer is 40 dynes/cm. This surface pressure corresponds to the difference between the surface tension of the water-air interface (68 dynes/cm) and the surface tension at the water-lipid interface. (For a clear explanation of the experiments see Jain, 1988, or Gennis, 1989.) So the surface tension at the water-lipid interface is estimated by this method to be 68–40, or 28 dynes/cm for the monolayer or 56 dynes/cm for the bilayer.

To relate the surface tension to the internal pressure, we utilize the following definition of the surface tension (Bakker, 1911; White, 1980):

$$\gamma = \int_{Z_1}^{Z_2} [P_N(Z) - P_T(Z)]\, dZ \qquad (1)$$

where γ is the surface tension, the z axis is normal to the plane of the membrane, P_N is the pressure normal to the membrane surface, P_T is the pressure tangent to the membrane surface and Z_2 and Z_1 are any positions along the z axis that bracket the interface. In the experimental conditions we are simulating, the mean value of P_N is 1 atmosphere. Substituting P_N = 1 atmosphere into Eq. 1 and rearranging:

$$\frac{\int_{Z_1}^{Z_2} P_T(Z)\, dZ}{(Z_2 - Z_1)} = 1 \text{ atm} - \frac{\gamma}{(Z_2 - Z_1)} \qquad (2)$$

The left-hand side of Eq. 2 is just the mean lateral pressure in the simulated system including the water-membrane interface. To evaluate this numerically, we estimate that our equilibrated hydrated preparation will have a thickness in the direction normal to the membrane plane (Z) of 55 Å. The appropriate negative lateral pressure for the boundary conditions is then given by the following value:

$$\begin{aligned}\text{boundary lateral pressure} &= 1 - \text{surface tension}/55\ \text{Å} \\ &= 1 - (56\ \text{dynes/cm})/55 \times 10^{-8}\text{cm} \\ &= \sim -10^8\ \text{dynes/cm}^2 \\ &= \sim -100\ \text{atmospheres.}\end{aligned}$$

On the basis of the above considerations, the lateral pressure for the simulations was set to −100 atmospheres, as shown schematically in Fig. 1 *C*. For the dimensions used in this simulation, the second term on the right-hand side of Eq. 2 dominates the determination of the lateral pressure. If the size of the box along the Z dimension were very large the first term on the right-hand side would dominate and the lateral pressure would just go to 1 atmosphere, but such a large box would not be feasible for computations.

The use of the mean pressure for the boundary condition does not imply that the lateral pressure is the same at the various depths within the preparation, but it is not necessary to deal with the spatial variation of the pressure to set the boundary condition correctly. The critical point here is that, for a three-dimensional region of space containing an interface, the fundamental definition of the surface tension is in terms of the mean lateral pressure according to Eqs. 1 and 2, rather than being defined in terms of the the lateral pressure at any particular position on the z axis. Because experimentally surface tension is always a macroscopic quantity measured by macroscopic means (White, 1980), the definition in terms of the mean lateral pressure as in Eqs. 1 and 2 is fundamental.

The coupling constant between the internal virial and the constant pressure boundary was taken to be 0.4 ps for the early part of the simulation (Berendsen et al., 1984). In the later part of the simulation, the constant was changed to 4 ps to reduce short-term fluctuations in the system dimensions.

After the simulated preparation was gradually heated to 325 K, 350 ps of continuous dynamics were run at 325 K. Detailed data analysis was done for two intervals, 80–140 ps and 300–350 ps. The results for both intervals were quite similar to each other and, as will be seen below, characteristic of a fluid phase membrane. The system was slowly changing its dimensions, having an area per lipid molecule of 56 Å^2 at 140 ps and 57.3 Å^2 at 350 ps. We judged that running the system to complete equilibration was prohibitive of computer time and unlikely to change the results significantly, so we are reporting in detail on the results of the system up to 350 ps. The configuration shown in Fig. 1 *C* is a snapshot of the system at an advanced stage of the computation, so the entire computation can be summarized as the evolution of the system from Fig. 1, *A* to *C*. This evolution involved a considerable change of dimension. The original configuration had an area/phospholipid molecule of 39 Å^2, whereas the final configuration had an area/phospholipid molecule of >57 Å^2.

RESULTS

The major results of the simulations are summed up pictorially in Fig. 2. This figure shows various aspects of a snapshot of a fluid phase hydrated DMPC membrane at the very end of our simulations, i.e., after 350 ps at 325 K. Fig. 2, *A–C*, shows parts of the system in isolation and Fig. 2 *D* shows the entire system. Fig. 2 *A* shows the water. It is seen that the water is present at bulk concentration outside the membrane and penetrates well into the interfacial region, albeit at reduced concentration at deeper levels. Fig. 2 *B* shows the polar regions of the phospholipids, from the

choline groups at the ends of the headgroups to the carbonyl groups at the heads of the hydrocarbon chains. Of interest is the roughness of the surface and the fact that the major axis of the headgroup from the phosphorus of the phosphate to the nitrogen of the choline group is, on the average, almost parallel to the membrane plane. Fig. 2 *C* shows just the hydrocarbon tails. It is seen that they are quite disordered. Each chain has a substantial mean tilt away from the bilayer normal, but there is little or no collective tilt of the whole assembly of chains. The density of the material becomes lower near the center of the bilayer. This is consistent with the packing patterns of liquid alkanes, where the methyl groups at the ends of the chains occupy substantially more volume per group than the methylene groups in the chain interiors (Nagle and Wiener, 1988). Fig. 2 *D* shows the full computed system (the parts of which are shown separately in Fig. 2, *A–C*) in one color-coded figure (orange for phospholipid headgroup atoms, blue for water oxygens, white for water hydrogens, and green for hydrocarbon tails). The structures of Fig. 2 show a tendency for occasional single phospholipid molecules to protrude from the surface of the bilayer. This is predicted theoretically (Israelachvili and Wennerstrom, 1992) and apparently contributes to the repulsive pressure between membranes at small intermembrane spacings (McIntosh et al., 1995).

To get valid statistics for numerical indices of the membrane's structure and behavior, conformations must be averaged over a period of time rather than inferred from an instantaneous conformation. In the results described below, the numerical values were time-averaged in the interval 300–350 ps of the simulation at the final temperature of 325 K. During the analysis time the dimensions of the system fluctuated slightly. The surface area/DMPC molecule fluctuated between 57.0 and 57.3 $Å^2$ and the size of the box normal to the membrane fluctuated between 55.8 and 56.3 Å.

One representation of the overall structure of the system is in the electron density profile. Fig. 3 shows the electron density profile along the bilayer normal axis in arbitrary units. In this calculation each of the heavy atoms C, O, P, and N are weighted by the atomic number plus the partial charge. The computed curve is in excellent agreement with corresponding experimental curves from McIntosh (1990).

Fig. 4 shows the structure and orientation of the hydrocarbon tails. Fig. 4 *A* represents one classic definition of the fluid phase membrane, the order parameters derived from NMR measurements on chains with deuterium labels on the ethylene groups at various positions in the hydrocarbon chains. The plot shows the CD order parameter, given by

$$S_{CD} = 0.5(3\langle\cos^2\theta\rangle - 1) \quad (3)$$

where θ is the angle between the C-D bond and the bilayer normal. Because we have no explicit nonpolar hydrogrens in the simulation, the positions of the deuterium atoms were reconstructed from the coordinates of the acyl chains, assuming ideal geometry of the C-D bond. The coordinates of both possible Ds for each C were reconstructed and both averaged in to give the final contribution to the order parameter. The order parameters shown in Fig. 4 *A* are computed from the same molecular dynamics trajectories as the electron density profile shown in Fig. 3. They have a similar form to experimentally measured order parameters for PC membranes (Oldfield et al., 1978; Rice and Oldfield,

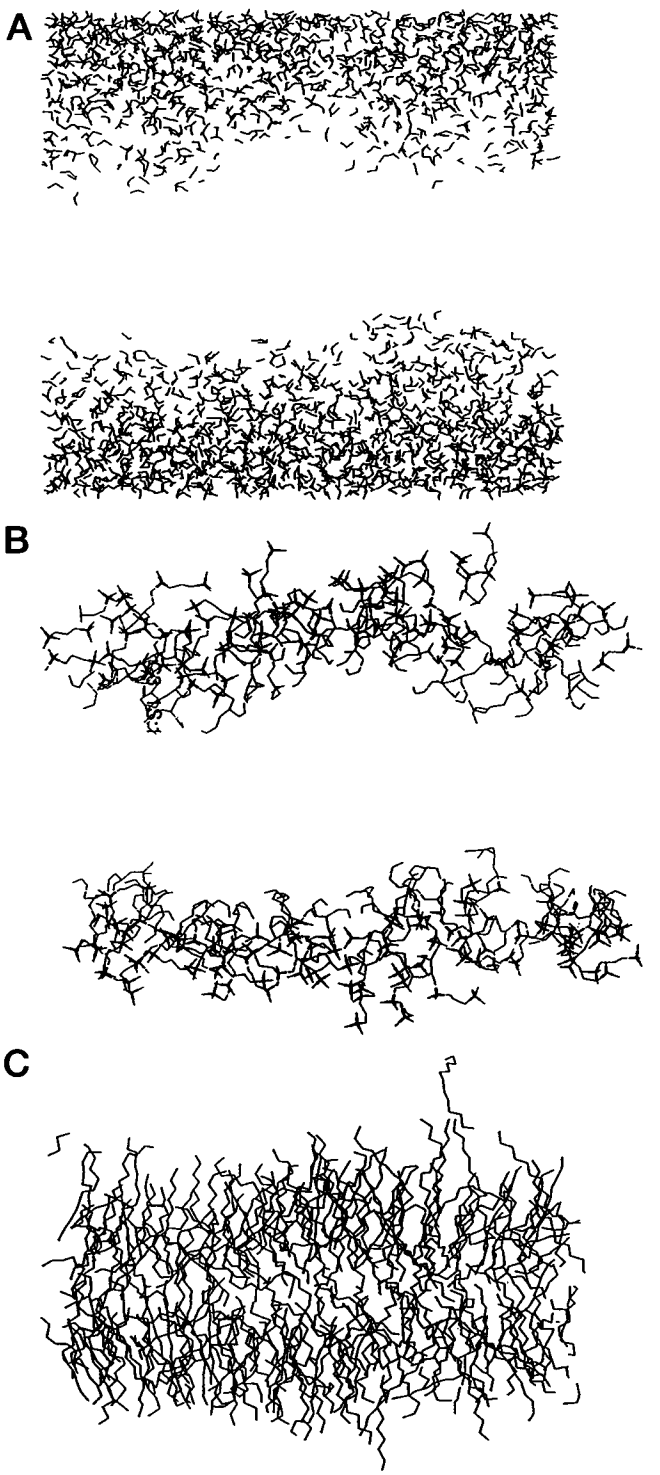

FIGURE 2 *A*, *B*, and *C*

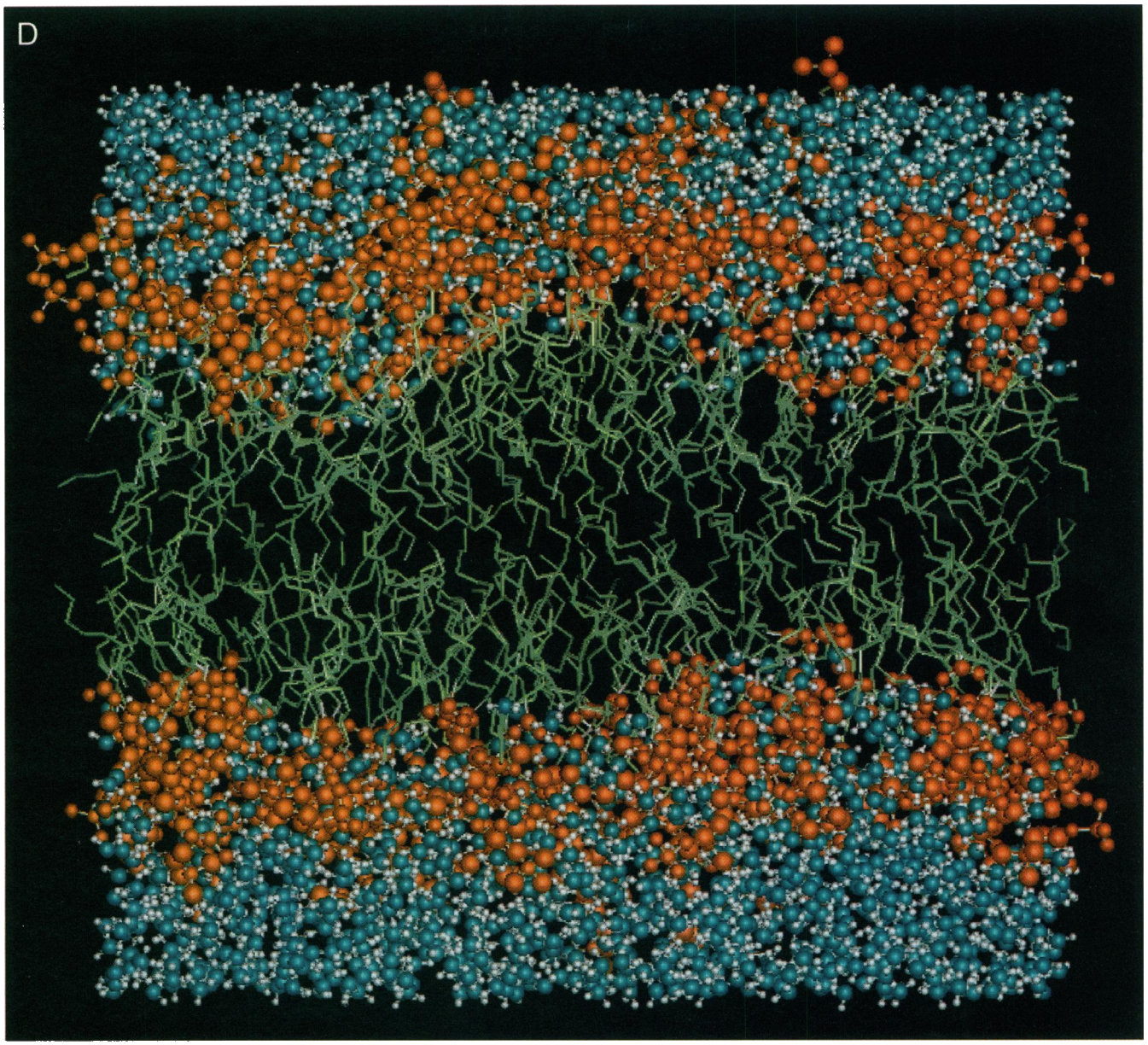

FIGURE 2 (*Continued*) Snapshot of system conformation at the end of the simulation. Different parts of the figure show components of the system, each at the same time. (*A*) Water, showing bulk concentration outside the membrane and penetration into the headgroup region, down to the carbonyl groups. (*B*) Polar regions of the phospholipid, from the choline groups at the ends of the headgroups to the carbonyl groups at the heads of the hydrocarbon chains. (*C*) Hydrocarbon tails of the phospholipids. (*D*) The entire system, consisting of *A*, *B*, and *C* depicted together. Color coding is as follows. Orange spheres are polar atoms of the phospholipid headgroups. Water oxygen atoms are blue. Water hydrogen atoms are white. Atomic spheres are less than full van der Waals size so that the reader may see somewhat into the structure to assess surface roughness and degree of water-lipid interpenetration. Hydrocarbon chains are green. Note that the visualization program distinguishes molecules according to charge groups. Thus when the first atom in a charge group is in the central box, the entire charge group is visualized even when it extends past the central box.

1979; Seelig and Seelig, 1980; McCabe et al., 1994). All results show a near plateau region near the tops of the chains, at an order parameter value near -0.2, and a precipitous drop near the center of the membrane.

It is also of interest to calculate the average $\langle P_4(\cos\theta)\rangle$ where P_4 is the fourth Legendre polynomial and θ is as defined above. Morrison and Bloom (1993, 1994) have derived equations for relaxation rates measured by deuterium magnetic resonance as functions of the angle between the bilayer normal and the static applied field. The parameters in these relations are themselves functions of $\langle P_2(\cos\theta)\rangle$ and $\langle P_4(\cos\theta)\rangle$. According to the assumptions made by Morrison and Bloom, the average $\langle P_4\rangle$ over all bonds in all chains must lie between 0 and $\sim$0.05. Fig. 4 *B* shows a profile of $\langle P_4\rangle$ calculated in the simulations. It is seen that the calculated $\langle P_4\rangle$ for all bonds lie within this range.

Fig. 4 *C* shows the distribution of dihedral angles in the hydrocarbon chains, both for the computed membrane (solid line) and also for the gas phase as predicted from the bare

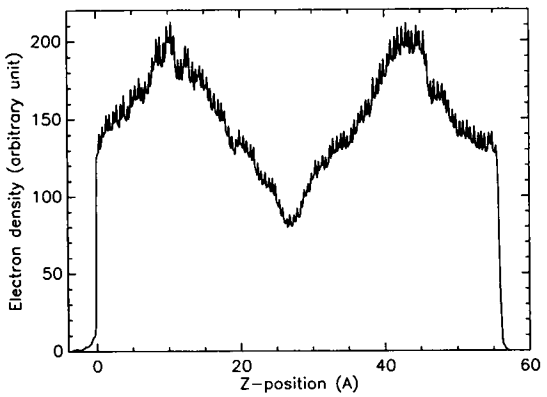

FIGURE 3 Electron density profile of the fluid membrane, averaged in the time interval 300–350 ps at the final temperature of 325 K. Close agreement is seen with experiments such as in McIntosh (1990).

Ryckaert-Bellemans potential (dashed line). It is seen that practically all of the dihedral angles are in the neighborhood of either the *trans* (0°C) or one of the two *gauche* (+ or −120°C) configurations. The simulated membrane has a slightly lower *gauche/trans* ratio than the gas phase prediction. In the simulated membrane, approximately one-fourth of the angles are in the neighborhood of one of the *gauche* configurations, in agreement with experiments on the closely analogous DPPC membrane (Mendelsohn and Senak, 1993). Fig. 4 *D* shows the time course of $g+$, $g-$, and t fractions during the 50 ps of data that were averaged to produce Fig. 4, *A–C*. It is seen that the *gauche/trans* ratio did not vary significantly during this period but that there was a slight drift in the ratio of $g+/g-$.

In addition to the overall incidence of *gauche* and *trans* bonds it is significant to tabulate the incidence of conformers consisting of sequences of different classes of bonds and compare them with experiment. Table 1 shows data from Fourier transform infrared spectroscopic (FTIR) studies of DPPC and dilauroylphosphatidylcholine from experiments by Casal and McElheney (1990) and Mendelsohn and Senak (1993). The FTIR method detects CH_2 wagging modes at different wavenumbers for end *gauche*, double *gauche*, and *gauche-trans-gauche* conformers (Snyder, 1967). Although there is difficulty in separating contribu-

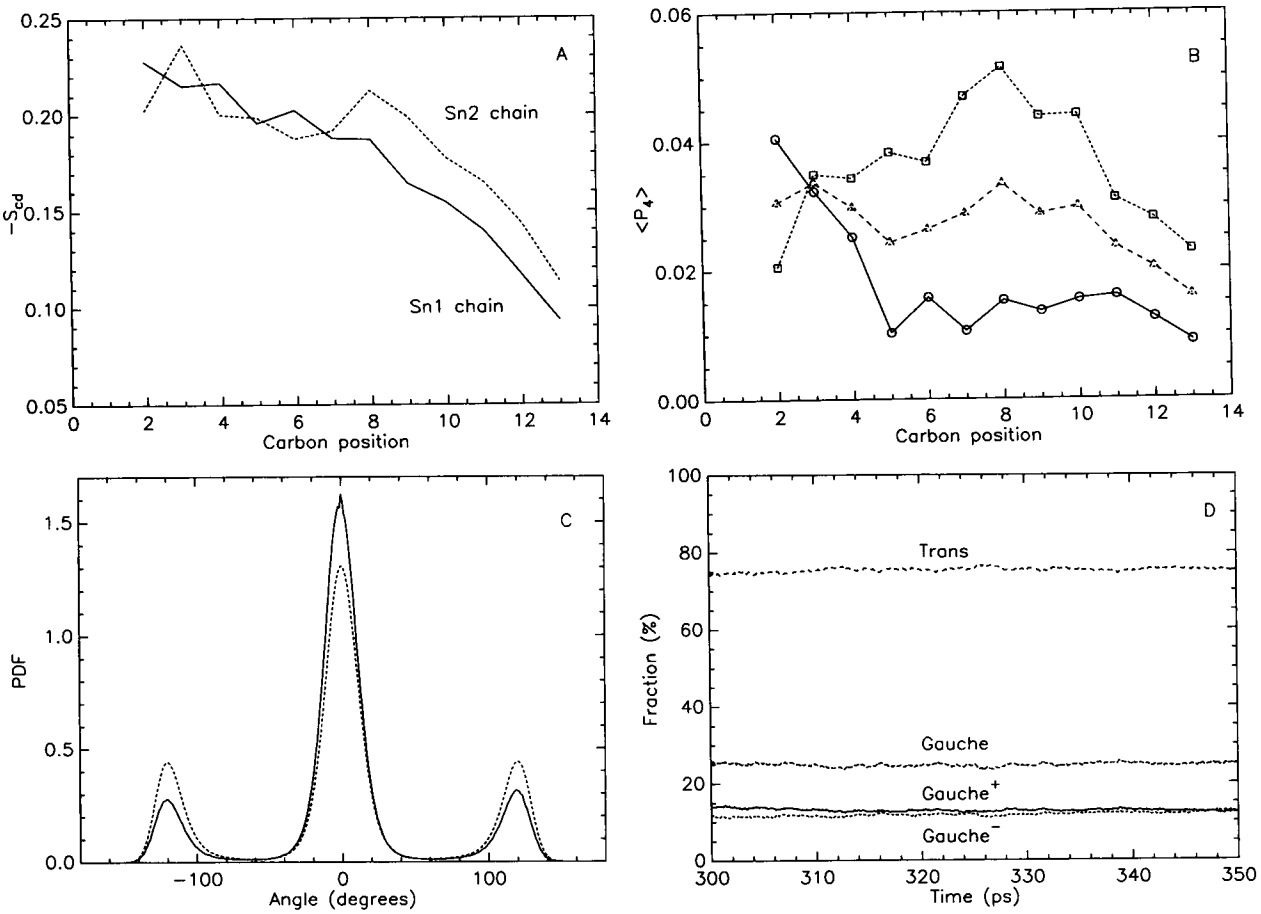

FIGURE 4 (*A*) Molecular order parameters of the computed membrane, averaged in the time interval 300–350 ps. (*B*) Profile of $\langle P_4(\cos\theta)\rangle$ (the fourth Legendre polynomial of the cosine of the molecular tilt angle) for the same data set as *A*. (*C*) Distribution of dihedral angles in the hydrocarbon chains. The dashed line is the distribution predicted from the bare Ryckaert-Bellemans potential and the solid line is that observed in the simulated membrane for the same data set as *A* and *B*. (*D*) Time course of the fraction of the bonds that are *trans*, *gauche+*, and *gauche−* during the simulated time for which the data in *A*, *B*, and *C* were collected.

TABLE 1 Comparison of simulation in this paper and published experiments for dihedral bond distributions

	Number of bonds or bond sequences per chain			
Bond type	Experimental DLPC*	Experimental DPPC*	Experimental DPPC‡	Simulation DMPC
end *g*	0.45	0.54	0.40	0.31
gg	0.32	0.40	0.40	0.34
gtg'	0.88	1.19		0.39
gtg' + *gtg*			1.00	0.67

*Casal and McElheney, 1990.
‡Mendelsohn and Senak, 1993.

tions from *gtg'* (kink) sequences and *gtg* sequences (Cates et al., 1994), the data provide an interesting test of the simulations. In the simulations, the numbers of end *gauche*, double *gauche* (*gg*), kink (*gtg'*), and *gtg* sequences were found by calculating all dihedral bond angles in the hydrocarbon chains in molecular dynamics configurations and averaging more than 1200 configurations, encompassing 80 ps of molecular dynamics. All bonds were classified as either *trans*, *g*+, or *g*−, according to whether the associated dihedral angle was closest to 0, +120, or −120°C, respectively. The computed result of double gauche bonds (*gg*) in Table 1 is in essentially complete agreement with experiment. The incidence of end *gauche* is somewhat lower than experiment. The fact that the *gg* fit is so much better than the end *g* fit suggests perhaps that the Ryckaert-Bellemans (1975, 1978) potential used for the hydrocarbon dihedral angles is not as valid for the end dihedral angle (which involves a CH_3 group) as it is for all the other dihedral angles that involve only CH_2 groups. (In the original Ryckaert-Bellemans work no distinction was drawn between the properties of the CH_2 and CH_3 groups.)

The simulations clearly show fewer *gtg* and *gtg'* incidences than is reported for experiment. However, there is greater uncertainty in the assignment of precise wavenumbers to *gtg'* and *gtg* CH_2 wagging modes in the FTIR experiments than there is for end *g* and *gg*. (Cates et al., 1994). This uncertainty is exemplified by the discrepancy between the data of Casal and McElheney (1990) and Mendelsohn and Senak (1993), as Casal and McElheney show larger values for *gtg'* alone than Mendelsohn and Senak show for *gtg'* plus *gtg*.

Fig. 5 shows histograms of the various atom types in the membrane along the bilayer normal. These are computed from the same data as Figs. 3 and 4. Fig. 5 *A* shows the variations in water penetration and hydrophobic thickness of the membrane. The region of water penetration, summed over the entire membrane face and over 50 ps, extends over ~20 Å. The distance to fall from 90% of bulk density to 10% of bulk density is 12–13 Å. This compares to a value of 10 Å for another computation of hydrated PC membrane with somewhat different parameters (Marrink et al., 1993). There is ~10 Å of overlap between the CH_2 and the water distributions. The deepest penetration of the water coincides with the position of the carbonyl oxygen nearest to the center of the membrane. This correspondence suggests that the water typically penetrates the membrane down to the carbonyl group. This is borne out by comparing Fig. 2, *A* and *B*, and can readily be seen in the color-coded visualization of the computed membrane in Fig. 2 *D*. Fig. 5 *B* shows the distributions of selected atoms from the phospholipid. It is seen that the phosphate and choline groups lie at almost the same depth in the membrane, showing that headgroups are oriented more parallel to the membrane plane than normal to it. The distribution curves for each atom, although noisy, would be reasonably approximated by Gaussian distributions with a half-width a bit under 10 Å. These features of the lipid-water interpenetration, membrane surface roughness, and headgroup orientations are very consistent with features derived from neutron and x-ray diffraction techniques on a PC membrane (Wiener and White, 1992b). However, in comparing the simulations with these particular experiments it should be noted that in the experimental situation the membrane was not as fully hydrated as in the simulation. The experimental system had only ~5 five water molecules per lipid molecule as opposed to the 21 in the simulation.

Another comparison with experiment is to the membrane width of fluid DMPC as measured by the mean P-P distance between the two membrane faces. This was measured by Lewis and Engleman (1983) to be 34 Å. The corresponding distance as shown in our data of Fig. 5 *B* is 35 Å.

Another measure of the hydration of the phospholipid is how many waters are in the first hydration shell of the phospholipid. Measurement of deuterated water NMR spin

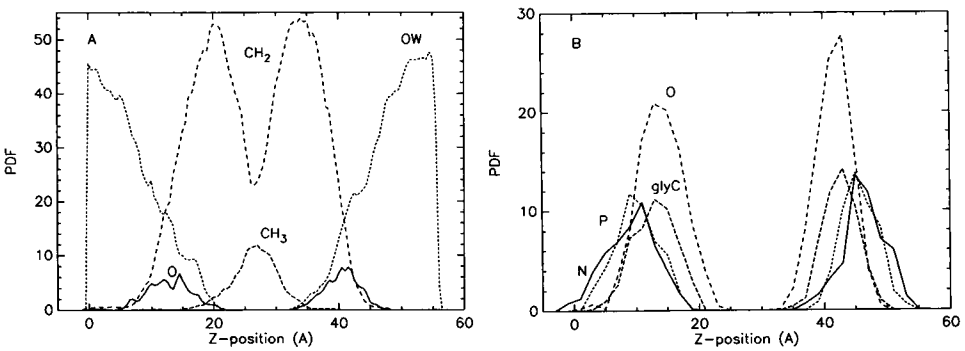

FIGURE 5 (*A*) Histogram of distribution of water, hydrocarbon groups, and carbonyl oxygen groups along the bilayer normal, for the same data set as Figs. 3 and 4. (*B*) Simulated distribution of position of polar atom types in the direction normal to the membrane plane, averaged over the same data set as *A*.

lattice relaxation time as a function of lipid hydration suggests that this number is ~11–16 waters per phospholipid molecule (Borle and Seelig, 1983). Fig. 6 shows a radial distribution function (RDF) of the distance to the nearest phospholipid headgroup atom for the population of water molecules in the simulation. The high peak represents the first layer of water molecules hydrating the phospholipid. Normally the definition of the first shell would be the number of waters found inside the radius corresponding to the first minimum after the main peak in the RDF. No such minumum is seen in Fig. 6 because the number of waters in the system is too small; yet the radial distribution function certainly goes out to distances beyond the first shell. In this situation we use an alternate definition, namely, that the first hydration layer comprises the distribution under the RDF curve up to one water radius from the leading edge (climbing phase) of the curve. The climbing phase of the RDF is over a range of 2.5–3 Å, so the first hydration shell is the water up to a distance of 4–4.5 Å. Also shown on Fig. 6 is the integral of the RDF curve. It shows that ~14 water molecules per phospholipid molecule are within 4–4.5 Å of some phospholipid headgroup atom, in good agreement with the NMR results, which put 11–16 waters in this region.

Fig. 7 shows the actual simulated area/phospholipid molecule versus that computed from a time series of instantaneous order parameters by the formula of Nagle (1993). The dashed line is the actual area obtained by dividing the area of the computational box by the number of phospholipid molecules, and the solid line is the area calculated from the order parameters by the Nagle formula. It is seen that the theoretical area is somewhat greater than the actual computed area. The actual computed area is ~57 Å^2 per phospholipid molecule, in agreement with the expectations from monolayer data (Albrecht et al., 1978; MacDonald and Simon, 1987). The theoretical area from the Nagle formula is ~62 Å^2 per phospholipid molecule.

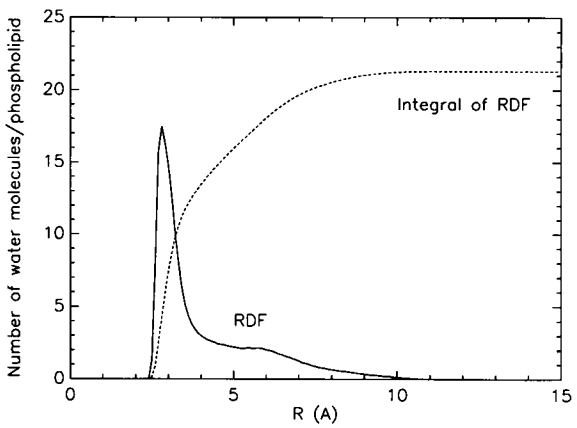

FIGURE 6 From same data set as Figs. 3–5. (*A*) Histogram of distance to the nearest phospholipid headgroup atom for the population of water molecules in the simulation. The high peak represents the first layer of water molecules hydrating the phospholipid. The first layer is approximately the distribution under the curve up to one water radius from the rising phase of the curve, or 4–4.5 Å. (*B*) Integral under *A*, showing that approximately 14 water molecules per phospholipid molecule are in the first hydration layer, in good agreement with the NMR results (Borle and Seelig, 1983).

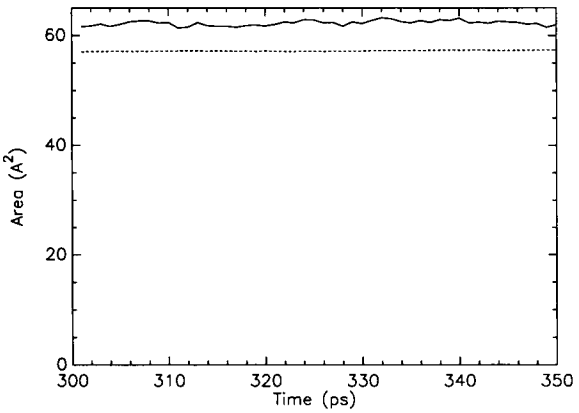

FIGURE 7 From same data set as Figs. 3–6. Simulated area/phospholipid molecule (dashed line) compared with the area/phospholipid predicted from the simulated order parameter profile by the formula of Nagle (1993) (solid line). It is seen that the simulated area is somewhat less than the theoretically predicted area. This suggests that previous estimates of the surface area/phospholipid for fluid PC membranes based on order parameters may be too high.

A possible reason for the discrepancy between the simulated and theoretical area is shown in Fig. 8. The data for Fig. 8 are time-averaged data about the density of carbon atoms in the strictly nonpolar center region of the membrane, where the only species are the methylene groups that make up the major part of the saturated chains and the methyl groups that are on the end of each chain. In Fig. 8, *A* and *B*, we show, respectively, the curves of the volume per carbon atom as a function of the distance along the bilayer normal and the fraction of the carbon that is in methylene groups versus the position along the bilayer normal. Fig. 8 *C* combines Fig. 8, *A* and *B*, to show the volume/carbon atom for the region near the center of the membrane, which is pure hydrocarbon versus the fraction of the carbon that is in methylene (as compared with methyl) groups. The straight line is the relationship that would pertain if the hydrocarbon were packed at precisely the same density as liquid alkanes, which is the assumption embodied in the Nagle (1993) relationship (Nagle and Wiener, 1988). It is seen that the volume/carbon atom near the top of the chains (near 100% CH_2) is somewhat lower than would be suggested by comparison with the liquid alkanes. This is the region that enters into the Nagle formulation. Thus it seems that the explanation for the difference between the simulated and theoretical predictions in Fig. 7 is that the sections of the chains near the polar regions in the simulated membrane pack more densely than the comparable liquid alkanes. This may relate to the fact that the membrane chains near the polar regions, although somewhat disordered, have some greater-than-random tendency to line up in parallel. Farther away from the polar regions

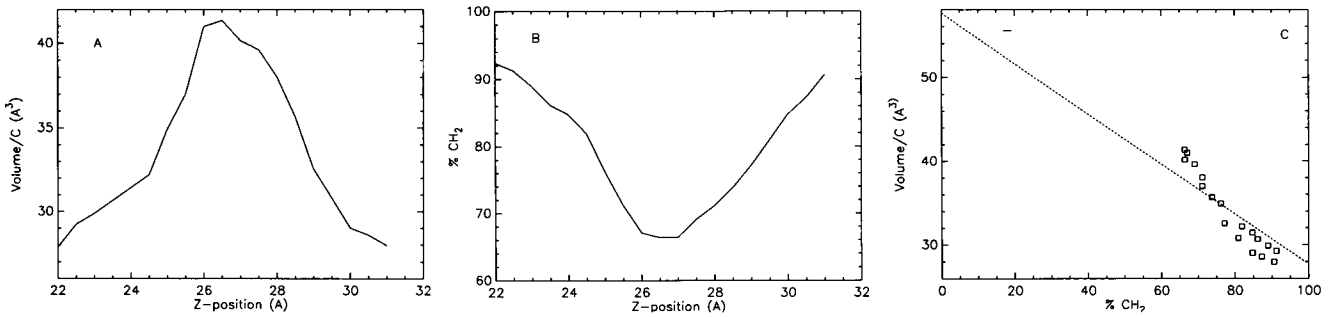

FIGURE 8 Possible explanation for the result shown in Fig. 7, based on the same data. This figure shows volume/carbon atom of the hydrophobic portion of the membane. (*A*) Volume/carbon atom as a function of the *z* coordinate (normal to the membrane plane). (*B*) Percentage of the carbon that is in methylene (as opposed to methyl) groups as a function of the *z* coordinate. This percentage is lowest in the center of the membrane because the groups at the ends of the hydrocarbon tails are methyls. (*C*) Plot of the dependent variables of *A* and *B* versus each other to show volume/carbon atom as function of the percentage of the carbon that is in methylene groups. The straight dashed line by comparison is the value that pertains for liquid alkanes at 40°C.

(lower percent CH_2), Fig. 8 *C* shows a somewhat less dense packing than the comparable liquid alkanes. We can think of two opposing tendencies in the bilayer that might account for the deviations of the density pattern from that of bulk alkanes shown in Fig. 8 *C*. On the one hand, the anisotropy of the interfacial situation tends to make the chains line up in parallel, giving more efficient packing and reducing the volume. On the other hand, the surface tension, being equivalent to a negative pressure in the plane of the membrane, will tend to increase the volume. We can also think of two aspects of the simulations that might lead to the the pattern of Fig. 8 *C*. One is that, at 350 ps at 325 K, the simulations may not be completely equilibrated and it might be that the fully equilibrated membrane would have an internal density profile just like liquid alkanes. Also, the density profile will be strongly influenced by the particular choice of van der Waals parameters for the CH_2 and CH_3 groups. But whether the discrepancy shown in Fig. 8 *C* is a result of the inherent physics of the bilayer or of the sensitivity of this measure to the simulation details, these are second order effects in the fluid phase membrane. To the first order, the situation is that the overall mean density of the hydrocarbon interior in our simulations is similar to that of liquid alkanes of comparable composition, consistent with earlier suggestions in the literature (Nagle and Wiener, 1988; Wiener and White, 1992a; Nagle, 1993).

It is of interest to examine water orientations and mobility in the interfacial region. Fig. 9 *A* shows the mean cosine of the angle between the water dipole moment and the bilayer normal. (Note that in all the sections of Fig. 9 the water between the membranes is at the center of the horizontal axis and the hydrocarbon interior is at the left and right sides of the graph. This was accomplished by translating all the coordinates in the *z* direction by one-half of the size of the central box and was done to avoid creating artifactual apparent polarizations at the box edges by how the waters at the edge were defined to be in or out of the box.) For water being randomly oriented, the value of the cosine in Fig. 9 *A* will be zero, so it is seen that the water in the interfacial region is selectively oriented in such a way as to make the interior of the membrane electrically positive relative to the bulk solution. This is qualitatively correct to account for the experimentally measured dipole potential, which has been shown for PC membranes to arise from water orientations in the interfacial region (Gawrisch et al., 1992). This degree of orientation is also very similar to that observed by Marrink et al. (1993) in a computation that had somewhat less complete hydration of the lipid (11.5 waters/lipid, rather than the 21 that we had.) Fig. 9, *B–D*, shows the basis for the dipole potential at the membrane surface. Fig. 9 *B* shows the charge density as a function of position in the dimension normal to the membrane plane for the water (short dashes), the lipid (long dashes), and the total of water plus lipid (solid line). Fig. 9 *C* is the negative of the first integral of the charge in Fig. 9 *B*, which gives the electric field. Fig. 9 *D* is the integral of the field in Fig. 9 *C*, which gives the electrostatic potential derived from the charge distribution of the water and the lipid and shows the computed potential profile across the membrane associated with water polarization and with phospholipid charge distribution. One striking feature of Fig. 9, *B–D*, is the smoothing effect of the successive integrations of the charge. It is difficult to discern by eye any pattern in the charge distribution in Fig. 9 *B*, but the pattern emerges strongly in the successive integrations to produce the patterned field in Fig. 9 *C* and the relatively smooth contributions to the potential profile from lipid and water in Fig. 9 *D*. (The corollary to the smoothing effect of integration is that differentiation produces noise, which is why differentiation is to be avoided when programming an analogue computer. The relationships between Fig. 9, *B–D*, demonstrate this point.) It is seen that the contributions to the total potential from the water and the lipid are opposite to each other and that the net potential (which is the only experimentally measurable quantity) is a relatively small difference between two large quantities. We also see evidence of limitations of the sampling in our data, in that the net potential differences caused by the lipid and the water separately are each almost a volt from one side to the other of the computational box. If the two halves of the bilayer were precisely symmetrical, these net voltage dif-

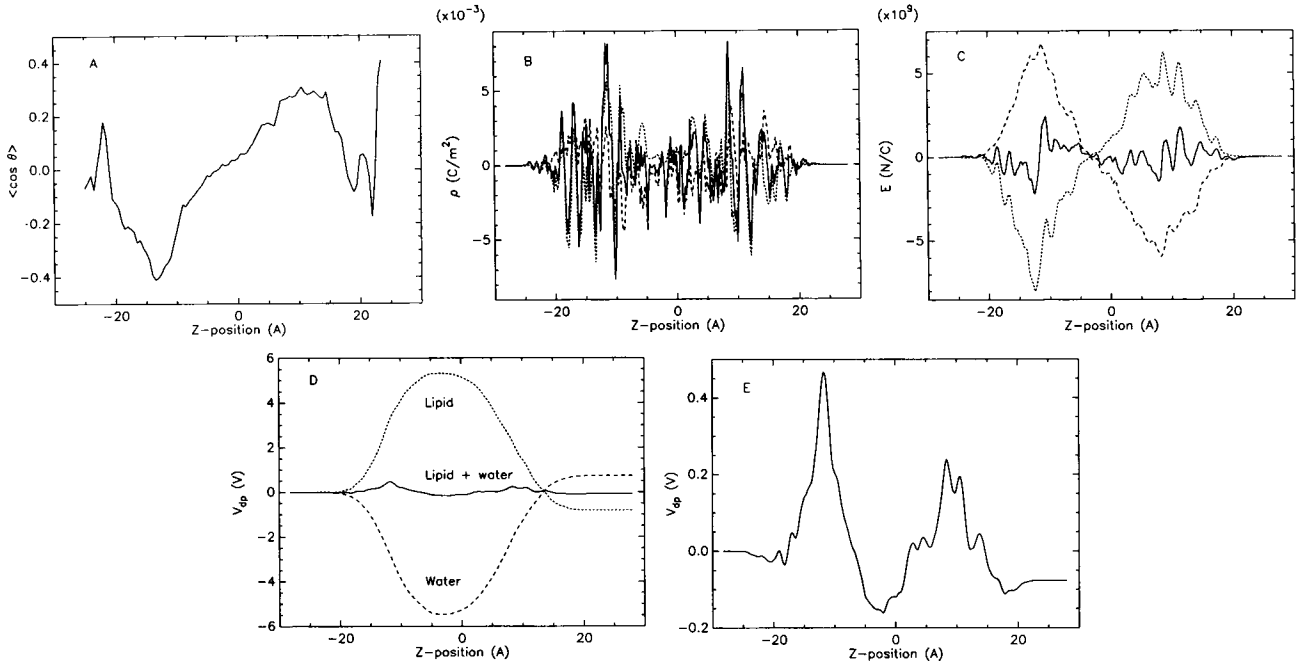

FIGURE 9 From same data set as Figs. 3–8. (*A*) Mean cosine of the angle between the water dipole moment vector and the axis normal to the membrane plane. It is seen that there is a strong tendency for the water dipole moment to point inwards toward the hydrocarbon region of the membrane. (*B–E*) Basis for the dipole potential. Note that in *B–E* the horizontal axis of the curves is shifted so that the center of the axis is in the aqueous region between opposing membrane faces. (*B*) Charge density as a function of position in the dimension normal to the membrane plane for the water (short dashes), the lipid (long dashes), and the total (water plus lipid). (*C*) Negative of the first integral of the charge in *B*, which gives the electric field. (*D*) Integral of the field in *C*, which gives the electrostatic potential derived from the charge distribution of the water and the lipid. (*E*) Total potential, including both the lipid and the water contributions, with an expanded vertical scale so that the detail can be seen. It is seen that there is a positive potential within the membrane relative to the bulk, in agreement with experiment. It is also seen that there is a potential barrier in the interfacial region.

ferences would be zero. As there is no methodological bias that would produce systematic assymetries between the two halves, the asymmetries in Fig. 9 *D* are a result of inadequate sampling, which would be corrected by having a longer computer simulation over which to average the results. To get a partial assessment of the limitations of sampling, we divided the 50-ps time series into 50 1-ps segments and also into 10 5-ps segments. This gave us a larger number of measurements from which we could calculate a standard deviation and probable error (standard deviation/$N^{0.5}$, where N is the number of different measurements) as well as a mean. The mean dipole potential and probable error with the 1-ps segments for the two sides of the membrane were 162 ± 22 mv and 99 ± 23 mv. With the 5-ps segments the corresponding results were 162 ± 27 mv and 99 ± 40 mv.

Fig. 9 *E* shows only the net potential profile, on a larger scale so the detail is more visible. The net dipole potential, from the fluid to the hydrocarbon interior, is ~162 mv on one side of the membrane and ~99 mv on the other side, for an average of ~130 mv. Comparison of this number with experiment will be given in the Discussion and Summary. In addition to a net dipole potential, Fig. 9 *E* also suggests that there is a substantial potential barrier of several hundred millivolts in the interfacial region on both sides of the membrane.

From Fig. 9 it appears that we do not have any water that can really be called bulk, so it is impossible to tell how far the potential extends into the fluid spacing. This is especially clear from Fig. 9 *A*, as in this figure a region of bulk water would appear as a horizontal region with the cosine equal to zero. The peaks in five different distributions correspond quite closely to each other. These are the total potential profile (Fig. 9 *E*), the degree of net orientation of the waters (Fig. 9 *A*), the distributions of phosphate phosphorus and choline nitrogen (Fig. 5 *B*), and total electron density (Fig. 3). On one side of these peaks, the electrolyte side, the field produced by the water orientations has a higher magnitude than that produced by the lipid, so the potential rises as one goes toward the center of the membrane. On the other side of the peaks, the side toward the hydrocarbon, the water is less dense and the field caused by the lipid orientations is of larger magnitude than that caused by the water, so the potential declines as one moves toward the membrane interior.

Fig. 10 provides information about the mobility of the water in the interfacial region. Fig. 10 *A* shows the mean square deviation correlation function (MSD) for water molecules at different depths in the membrane-water interfacial region. The defining equation is:

$$\mathrm{MSD}(\tau) = \langle(\mathrm{r}(t + \tau) - \mathrm{r}(t))^2\rangle$$

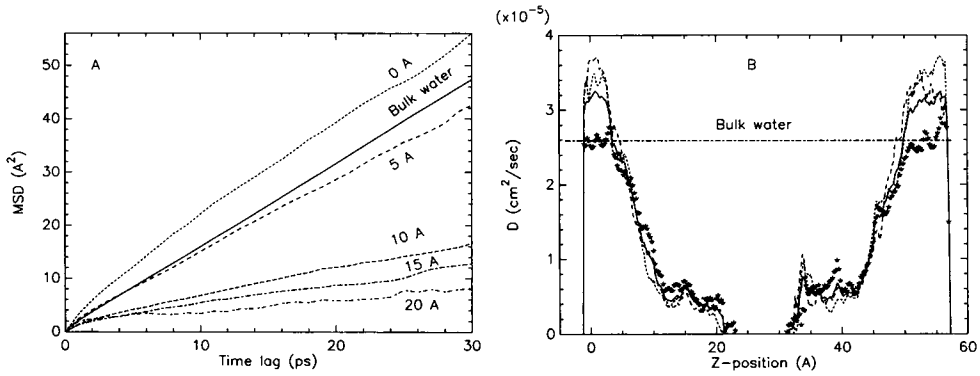

FIGURE 10 From same data set as Figs. 3–9. (*A*) Mean square deviation correlation function for water molecules at different depths in the membrane and also for bulk water using the same water model (SPC/E). (*B*) Diffusion coefficient of the water, as a function of position along the bilayer normal. The determination was made with a 20-ps correlation time, for the *x*, *y*, and *z* axes separately. Dashed curves are for the *x* and *y* dimensions, the asterisk is for the *z* dimension, and the solid curve is for the mean of the three dimensions. The horizontal dashed line for comparison purposes is the value computed for the SPC/E water model in a bulk simulation and is also very close to the experimental value for the self-diffusion coefficient for water.

In each case the population of water molecules at time *t* consists of those from a bin of 1-Å width from the indicated position, 0, 5, 10, 15, and 20 Å. Thus the 0-Å curve is from the water farthest from the center of the membrane and the 20-Å curve is from deep within the membrane, near the boundary between the interfacial region and the hydrocarbon tails. It is seen that the diffusion coefficient (defined as one-sixth of the slope of the MSD) decreases steadily as one goes deeper into the membrane. For comparison we also show the MSD for a computation done in our laboratory of a box of water molecules using the same water model, SPC/E. This curve is labeled bulk. It is seen that the water at the surface of the membrane is not bulk-like but actually has a diffusion coefficient greater than bulk. Another measure of whether the water at the surface of our computational box is bulk-like is shown in Fig. 10 *B*, where we look at the degree of anisotropy in the diffusion. In this curve the MSD is computed separately in the *x*, *y*, and *z* directions. The diffusion coefficient is calculated from the MSD with a 20-ps time lag for each dimension separately and plotted separately, with the dashed lines indicating the *x* and *y* dimensions and the asterisk indicating the *z* dimension. It is seen that at the surface of the computational box the water mobility is greater in the *x* and *y* directions (in the plane of the membrane) than the mobility for bulk water, whereas in the *z* direction (normal to the membrane plane) the water mobility at the surface is approximately equal to that of bulk water. Because the water nominally outside the membrane is not diffusing isotropically, it seems that the 21 waters/lipid molecule in the system falls short of being excess water, or full hydration. The significance of this finding is in the context that all of the experimental measures of the dipole potential are in conditions of excess hydration (Flewelling and Hubbell, 1986). For our smaller hydration and especially with periodic boundary conditions, our situation may be different in such a way as to affect the degree of water orientation. This point will be discussed further in the Discussion and Summary.

DISCUSSION AND SUMMARY

The major finding of this paper is that it demonstrates that a fluid phase hydrated lipid bilayer membrane can be simulated without incorporating into the simulations any arbitrary or artificial bias toward fluidity. The demonstration consists of a simulation in which the starting configuration for the lipid bilayer was the x-ray crystal structure and the phospholipid molecules had full partial charges as calculated by an ab initio SCF calculation. After heating, the simulated system adopted conformations characteristic of the fluid state, as shown by hydrocarbon tail order parameters and distribution of headgroup atoms. The major new technique used to achieve this result was to take into account the surface tension at the water-membrane interface. This was done by doing the computations with periodic anisotropic constant pressure boundary conditions. The pressure in the direction normal to the membrane plane was 1 atmosphere, representing the laboratory environment. A negative pressure of −100 atmospheres was applied in the membrane plane, representing the surface tension.

Compared with other simulations of lipid bilayers, the major advance in this paper is that the surface area per lipid molecule and the membrane fluidity emerge from the detailed force field of the molecules in the system plus boundary conditions that correspond to the laboratory pressure and the surface tension in the plane of the membrane. Previous simulations of PC fluid membranes using periodic boundary conditions with constant volume (Venable et al., 1993; Alper et al., 1993a,b; Damodaran and Merz, 1994; Robinson et al., 1994) produced fluidity by requiring the area/phospholipid to be so large (typically ~65 Å^2) that the hydrocarbon chains became disordered by virtue of having a lot of room to move around in. Previous simulations with periodic boundary conditions with constant pressure (Egberts, 1988; Berendsen et al., 1992; Marrink et al., 1993; Egberts et al., 1994) produced a gel phase above the transition temperature unless the partial charges on the phos-

pholipid molecules were arbitrarily reduced. The present work shows that the molecular force fields used in molecular dynamics produce a fluid phase with no a priori assumption about the density of phospholipid in the membrane, provided that the boundary conditions take the surface tension into account.

This work also advances knowledge on PC membranes in showing that the orientations of the partial charges of the phospholipid and the water in a well hydrated membrane give rise to a dipole potential at the electrolyte interface of the same sign and similar magnitude to that observed experimentally. It had been shown some time ago that water oriented with dangling hydrogens preferentially oriented toward a hydrophobic surface (Lee et al., 1984). Other workers have noted that the water was oriented with dipoles preferentially facing toward the hydrocarbon interior in the interfacial region of a simulated PC membrane (Chiu et al., 1992; Alper et al., 1993b; Marrink et al., 1993; Damodaran and Merz, 1994). In our simulations and in those of others the polar headgroups tend to make the inside of the bilayer negative because of the orientation of the phosphate-choline dipole; the choline group on the average is slightly closer to the bulk water and the phosphate group is slightly closer to the hydrocarbon interior. In our simulations the polarization of the phospholipid is overbalanced by that of the water, so that the net polarization is such as to make the membrane interior positive relative to the bulk solution. It is not clear how much of the water polarization is a result of specific hydrogen bonding with the phospholipid or how much is the more generalized dangling hydrogen effect associated with water at a hydrophobic surface.

Zhou and Schulten (1995) simulated the dipole potential in a dilauroylphosphatidylethanolamine membrane. Their results were generally similar to ours in that the total dipole potential was the difference between oppositely directed potentials caused by the lipid and the water, with the water potential positive, the lipid potential negative, and the net potential positive.

The simulations were tested against many experimental measures of the structure of fluid membranes, such as order parameters, surface roughness, amount of water associated with the phospholipid, electron density profile, distribution of *trans* and *gauche* bonds, thickness of the membrane, and dipole potential. Agreement in general was very good.

With respect to the dipole potential, in addition to the sampling issues noted in Results, it should be pointed out that these results involved the use of a cutoff. However, the cutoff was group based and relatively long (20 Å). Also, all the charges in the system are in neutral charge groups situated in the high dielectric (and therefore well shielded) interfacial and aqueous regions. In another computational study of a similar membrane system, Alper et al. (1993a,b) tested the results of different cutoffs and concluded that a residue-based cutoff of 18 Å was long enough to eliminate significant errors. Based on these factors we believe our results are not substantially compromised by the cutoff we used, but a definitive conclusion relative to that point would require doing the simulations with an even longer cutoff or with another method altogether, such as Ewald sums, to see whether the same results were achieved.

With respect to the dipole potential, our results provide support for previous suggestions in the literature that the primary basis of the dipole potential in PC membranes is the orientation of water molecules in the interfacial region (Gawrisch et al., 1992; Chiu et al., 1992; Zheng and Vanderkooi, 1992). However, it might be more accurate, on the basis of Fig. 9, to say that the basis for the dipole potential is a subtle imbalance between the water orientations and the phospholipid headgroup orientations. Our computed dipole potential of 99–162 mv was less than reported experimental values. There are two types of experiments with which to compare our results. One is the measured potential across a PC monolayer at an air-water interface. This measurement typically results in a potential of the order of 400 mv, for example, 441 mv reported by Hladky and Haydon (1973) and 390 and 440 mv (for different hydrocarbon tails) reported by Pickar and Benz (1978). A second type of determination is to infer the potential from the differential membrane conductance induced by organic cations. This type of measurement results in a potential of the order of 200 mv, for example, 197 and 224 mv reported by Pickar and Benz (1978), 240 mv reported by Flewelling and Hubbell (1986), and 227 mv reported by Gawrisch et al. (1992). The reason for the discrepancy between these two types of results is not known. From our simulations and analysis we can say that this discrepancy is equivalent to a change of the mean interfacial water dipole orientation angle of $\sim 1°$ with respect to the bilayer normal. Thus very subtle orientational changes in a membrane system can result in enormous differences in electrical potential. Our simulated values of dipole potential (99 and 162 mv) are a bit lower than either type of experiment. In making this comparison it is important to note that the experimental determinations of this potential are in conditions of excess hydration. On the basis of our water mobilities shown in Fig. 10, we do not believe the excess hydration condition pertained in our simulation. A particularly relevant point here is that, because of the periodic boundary conditions, the distance between the opposing membrane faces in our simulation is within the range of the hydration pressure (McIntosh and Simon, 1994). It is known that the magnitude of the hydration pressure between closely opposed bilayers is correlated with the magnitude of the dipole potential in the fully hydrated bilayer of the same species of phospholipid (Simon and McIntosh, 1989). It follows that close opposition of membranes within the range of the hydration pressure is likely to change the degree of water orientation that contributes to the dipole potential. It will be of interest to do these simulations with more water molecules, hence a bigger distance between opposing membrane faces, to see whether that would affect the magnitude of the dipole potential.

In addition to the dipole potential, another noteworthy feature of the potential profile across the membrane is the

presence of potential barriers for the movement of positive charge across the interfacial region (Fig. 9 *E*). These barriers might be an explanation for the positive inside rule, which refers to the fact that a series of positively charged amino acids is a common stop signal for the insertion of proteins into membranes (von Heijne, 1994).

There are several possible hypotheses for why the water is less mobile the deeper one goes into the interfacial region. One hypothesis is that the water mobility is inhibited by the surrounding lipid, which is inherently less mobile than water. This hypothesis starts from the experimental observation that water molecules are inherently more mobile than phospholipid molecules, as exemplified by the experimental fact that the self-diffusion coefficient of water (2.5×10^{-5} cm^2/s) is several orders of magnitude larger than the self-diffusion coefficient of phospholipids in a phospholipid vesicle membrane ($\sim 10^{-8}$ cm^2/s) (Edidin, 1981; Jacobson, 1983). We also note that the diffusion coefficient of water in protein channels is strongly influenced by the protein mobility. We have observed this in simulations with gramicidin channels (Chiu et al., 1991, 1992) and with models of sodium channels (Sudhakar et al., 1995) in which we artificially reduced the mobility of the protein and saw that the mobility of the water in the channel was dramatically reduced. Finally note that the molecular ratio of water/lipid declines steadily as one penetrates more deeply into the interfacial region from the aqueous region (from Fig. 5, *A* and *B*), pretty much in parallel with the decline in the water mobility (Fig. 10 *B*). Combining these observations, we suggest that the water mobility reduction as one goes deeper into the interfacial region arises from the fact that the deeper waters interact more with lipid (relatively slowly moving) than with other waters (which are relatively rapidly moving). Another possibility is that the decline in water mobility is associated with the water structure being highly ordered. By one measure of ordering, the mean projection of the water dipole moments on the normal to the plane of the membrane (Fig. 9 *A*), the depths of maximal ordering correspond to a near (but not absolute) minimum in water mobility. One might also suppose that the water mobility would be lower in regions of higher overall material density. Comparing Fig. 3 (electron density) with Figs. 9 *A* and 10 *B*, it seems that the peaks in electron density correspond very closely to the positions of maximal water ordering and also correspond to a near minimum in water mobility. From the above it seems plausible that several factors, including density of surrounding material, mobility of surrounding material, and ordered structure of water, are involved in determining the water mobility and how it varies with position in the interfacial region. It should be noted that, according to Marrink and Berendsen (1994), the water mobility increases markedly when the water enters the middle of the membrane, presumably as a result of the reduced density in that region (Fig. 3) and to the inability of the nonpolar hydrocarbon chains to make hydrogen bonds with the water molecules.

A noteworthy result of our simulations is the area per phospholipid molecule that we find associated with the fluid phase (Fig. 7), which at less than 60 $Å^2$ is somewhat lower than is often suggested in the literature for PC bilayers (Janiak et al., 1979; Hauser et al., 1981; Lis et al., 1982; Lewis and Engleman, 1983; Albon, 1985). Our area arose from a boundary condition derived from the monolayer data of Albrecht et al. (1978). In those data the surface area per PC molecule for the fluid monolayer at the surface pressure that gives a phase change at the same temperature as the bilayer is less than 60 $Å^2$. MacDonald and Simon (1987) also argue, from measurements on monolayers and bilayers in equilibrium with each other, that fluid phase bilayer PC membranes, and the monolayers with which they are in equilibrium, have a surface area per PC molecule of less than 60 $Å^2$.

The precise surface tension is somewhat uncertain. MacDonald and Simon (1987) estimate the surface tension in the DMPC bilayer to be 23 dynes/cm, rather than the 28 dynes/cm used in our simulation. This would lead to a lateral pressure of ~ -80 atmospheres rather than the -100 atmospheres we used. Other workers have reported monolayer surface pressure in equilibrium with bilayers of 32 dynes/cm (Seelig, 1987; Portlock et al., 1992). These would correspond to a surface tension of 36 dynes/cm. They were observed with the anesthetic dibucaine and a signal peptide sequence in the membrane, respectively. Within the variation, there is agreement that the surface tension for a monolayer that corresponds to a bilayer is of the order of a couple or a few tens of dynes/cm. The variation may be caused by different lipids and different other molecules embedded in the lipid.

Because our simulations use a surface tension boundary condition derived from monolayers and result in a realistic fluid bilayer, our simulations support the concept that a bilayer is a close approximation to two monolayers, provided that the comparison is made at the corresponding temperature and surface tension and temperature (MacDonald and Simon, 1987).

Of interest in the future is to vary the degree of hydration of the membrane to estimate the sensitivity of membrane structure to this variable. Another useful exploration would be to test the sensitivity of the surface area/lipid of the simulated membrane against the magnitude of the postulated surface tension (represented in the simulations by the magnitude of the negative pressure in the membrane plane). Also, we now have sufficient confidence in the essential physical validity of the simulations to begin considering the interaction of peptides and other molecules with the membrane.

The simulations reported in this paper took many months to perform. We anticipate future results to be obtained more rapidly with the development of versions of GROMOS capable of efficiently exploiting the newest shared memory parallel supercomputers, such as the Silicon Graphics Power Challenge and the Convex Exemplar (Clark et al., 1994; Kufrin and Subramaniam, manuscript in preparation).

We presented the basic idea of using negative lateral pressure to emulate the surface tension, plus early simulations and analysis, at the 1994 Biophysical Society meetings, the 1994 Jerusalem Conference on Biochemistry, and the 1994 meeting on numerical algorithms in biomolecular simulations at the University of Kansas. By discussions at meetings we have become aware that a similar algorithm is being developed by R. Pastor and B. Brooks. We also had useful discussions with many other participants at those meetings and individually with S. Simon, J. F. Nagle, M. Bloom, and R. G. Snyder. S. White pointed out to us the definition of the surface tension in terms of the integrated lateral pressure in Eq. 1. C. Zheng kindly shared with us a coordinate file for the repeating subunit of the PC membrane x-ray crystal structure that was used in constructing the initial conformation for the simulations.

This work was supported by a grant from the National Science Foundation. Computations were done on machines at the Pittsburgh Supercomputing Center and the National Center for Supercomputing Applications.

REFERENCES

Albon, N. 1985. Transition and molecular packing in highly purified 1,2-dipalmitoylphosphatidylcholine-water phases. III. Structures of phases with high water content. *J. Phys. Chem.* 89:3147–3151.

Albrecht, O., Gruler, H., and E. Sackman. 1978. Polymorphism of phospholipid bilayers. *J. Physique*. 39:301–313.

Alper, H. E., D. Bassolino, and T. R. Stouch. 1993a. Computer simulation of a phospholipid monolayer-water system: the influence of long range forces on water structure and dynamics. *J. Chem. Phys.* 98:9798–9807.

Alper, H. E., D. Bassolino-Klimas, and T. R. Stouch. 1993b. The limiting behavior of water hydrating a phospholipid monolayer: a computer simulation study. *J. Chem. Phys.* 99:5547–5559.

Bakker, G. 1911. Theorie de la Couche Capillaire Plane dans les Corps Purs. Gauthier-Villars, Paris.

Berendsen, H. J. C., J. P. M. Postma, van W. F. Gunsteren, A. DiNola, and J. R. Haak. 1984. Molecular dynamics with coupling to an external bath. *J. Chem. Phys.* 81:3684–3689.

Berendsen, H. J. C., J. R. Grigera, and T. P. Straatsma. 1987. The missing term in effective pair potentials. *J. Chem. Phys.* 91:6289–6291.

Berendsen, H. J. C., B. Egberts, S.-J. Marrink, and P. Ahlstrom. 1992. Molecular dynamics simulations of phospholipid membranes and their interaction with phospholipase A_2. *In* Membrane Proteins: Structures, Interactions and Models. A. Pullman, J. Jortner, and B. Pullman, editors. Kluwer Academic Publishers, Amsterdam, The Netherlands. 457–470.

Board, J. A. Jr., J. W. Causey, J. F. Leathrum, Jr., A. Windemuth, and K. Schulten. 1992. Accelerated molecular dynamics simulation with the parallel fast multipole algorithm. *Chem. Phys. Lett.* 198:89.

Borle, F., and J. Seelig. 1983. Hydration of *Escherichia coli* lipids: deuterium T_1 relaxation time studies of phosphatidylglycerol, phosphatidylethanolamine and phosphatidylcholine. *Biochim. Biophys. Acta.* 735: 131–136.

Casal, L., and R. McElheney. 1990. Quantitative determination of hydrocarbon chain conformational order in bilayers of saturated phosphatidylcholines of various chain lengths by Fourier transform infrared spectroscopy. *Biochemistry.* 29:5423–5427.

Cates, D. A., H. L. Strauss, and R. G. Snyder. 1994. Vibrational modes of liquid *n*-alkanes: simulated isotropic Raman spectra and band progressions for C_5H_{12}-$C_{20}H_{42}$ and $C_{16}D_{34}$. *J. Phys. Chem.* 98:4482–4488.

Chiu, S. W., E. Jakobsson, S. Subramaniam, and J. A. McCammon. 1991. Time-correlation analysis of simulated water motion in flexible and rigid gramicidin channels. *Biophys. J.* 60:273–285.

Chiu, S. W., K. Gulukota, and E. Jakobsson. 1992. Computational approaches to understanding the ion channel-lipid system. *In* Membrane Proteins: Structures, Interactions and Models. A. Pullman, J. Jortner, and B. Pullman, editors. Kluwer Academic Publishers, Amsterdam, The Netherlands. 315–338.

Clark, T. W., R. v. Hanxleden, J. A. McCammon, and L. R. Scott. 1994. Parallelizing molecular dynamics using spatial decomposition. *Proc. Scalable High Performance Comput. Conf.,* Knoxville, TN.

Damodaran, K. V., and K. M. Merz. 1994. A comparison of DMPC- and DLPE-based lipid bilayers. *Biophys. J.* 66:1076–1087.

Darden, T., D. York, and L. Pedersen. 1993. Particle mesh Ewald: An *N*log(*N*) method for Ewald sums in large systems. *J. Chem. Phys.* 98:10089–10092.

Edidin, M. 1981. Molecular motions and membrane organization and function. *In* Membrane Structure. J. B. Finean and R. H. Michell, editors. Elsevier, New York. 37–82.

Egberts, E. 1988. Molecular dynamics simulations of multibilayer membranes. Ph.D. thesis, University of Groningen, Groningen, The Netherlands. 139 pp.

Egberts, E., S. J. Marrink, and H. J. C. Berendsen. 1994. Molecular dynamics simulation of a phospholipid membrane. *Eur. Biophys. J.* 22:423–436.

Flewelling, R. F., and W. L. Hubbell. 1986. The membrane dipole potential in a total membrane potential model: applications to hydrophobic ion interactions with membranes. *Biophys. J.* 49:541–552.

Gawrisch, K., D. Ruston, J. Zimmerberg, V. A. Parsegian, R. P. Rand, and N. Fuller. 1992. Membrane dipole potentials, hydration forces, and the ordering of water at membrane surfaces. *Biophys. J.* 61:1213–1223.

Gennis, R. B. 1989. Biomembranes: Molecular Structure and Function. Springer-Verlag, New York.

Hauser, H., I. Pascher, R. H. Pearson, and S. Sundell. 1981. Preferred conformation and molecular packing of phosphatidylethanolamine and phosphatidylcholine. *Biochim. Biophys. Acta.* 650:21–51.

Helfrich, P., and E. Jakobsson. 1990. Calculation of deformation energies and conformations in lipid membranes containing gramicidin channels. *Biophys. J.* 57:1075–1084.

Heller, H., M. Schaefer, and K. Schulten. 1993. Molecular dynamics simulation of a bilayer of 200 lipids in the gel and in the liquid-crystal phases. *J. Phys. Chem.* 97:8343–8360.

Hermans, J., H. J. C. Berendsen, W. F. van Gunsteren, and J. P. M. Postma. 1984. A consistent empirical potential for protein-water interactions. *Biopolymers.* 23:1513–1518.

Hladky, S. B., and D. A. Haydon. 1973. Membrane conductance and surface potential. *Biochim. Biophys. Acta.* 318:464–468.

Huang, P., J. J. Perez, and G. H. Loew. 1994. Molecular dynamics simulations of phospholipid bilayers. *J. Biomol. Struct. Dyn.* 11: 927–956.

Israelachvili, J. N., S. Marcelja, and R. G. Horn. 1980. Physical principles of membrane organization. *Q. Rev. Biophys.* 13:121–200.

Israelachvili J. N., and H. Wennerstrom. 1992. Entropic forces between amphiphilic surfaces in liquids. *J. Phys. Chem.* 96:520–531.

Jacobson, K. 1983. Lateral diffusion in membranes. *Cell Motil.* 3:367–373.

Jain, M. K. 1988. Introduction to Biological Membranes. John Wiley and Sons, New York.

Janiak, M. J., D. M. Small, and G. G. Shipley. 1979. Temperature and compositional dependence of the structure of hydrated dimyristol lecithin. *J. Biol. Chem.* 254:6068–6078.

Lee, C. Y., J. A. McCammon, and P. J. Rossky. 1984. The structure of liquid water at an extended hydrophobic surface. *J. Chem. Phys.* 80: 4448–4455.

Lewis, B. A., and D. M. Engleman. 1983. Lipid bilayer thickness varies linearly with acyl chain length in fluid phosphatidylcholine vesicles. *J. Mol. Biol.* 166:211–217.

Lis, L. J., M. McAlister, N. Fuller, R. P. Rand, and V. A. Parsegian. 1982. Interactions between neutral phospholipid membranes. *Biophys. J.* 37: 657–666.

MacDonald, R. C., and S. A. Simon. 1987. Lipid monolayer states and their relation to bilayers. *Proc. Natl. Acad. Sci. USA.* 84:4089–4093.

Marrink, S. J., and H. J. C. Berendsen. 1994. Simulation of water transport through a lipid membrane. *J. Phys. Chem.* 98:4155–4168.

Marrink, S. J., M. Berkowitz, and H. J. C. Berendsen. 1993. Molecular dynamics simulation of a membrane water interface: the ordering of water and its relation to the hydration force. *Langmuir.* 9:3122–3131.

McCabe, M. A., G. L. Griffith, W. D. Ehringer, W. Stillwell, and S. R. Wassall. 1994. H-2 NMR studies of isomeric omega-3 and omega-6 polyunsaturated phospholipid membranes. *Biochemistry.* 33:7203–7210.

McIntosh, T. J. 1990. X-ray diffraction analysis of membrane lipids. *In* Molecular Description of Biological Membranes by Computer Aided Conformational Analysis. R. Brasseur, editor. CRC Press, Boca Raton, FL.

McIntosh, T. J., and S. A. Simon. 1994. Hydration and steric pressures between phsopholipid bilayers. *Annu. Rev. Biophys. Biomol. Struct.* 23:27–51.

McIntosh, T. J., S. Advani, R. E. Burton, D. V. Zhelev, D. Needham, and S. A. Simon. 1995. Experimental tests for protrusion and undulation pressures in phospholipid bilayers. *Biochemistry.* 34:8520–8532.

Mendelsohn, R., and L. Senak. 1993. Quantitative determination of conformational disorder in biological membranes by FTIR spectroscopy. *In* Biomolecular Spectroscopy. R. J. R. Clark and R. E. Heister, editors. Wiley, New York. 339–380.

Morrison, C., and M. Bloom. 1993. General orientation dependence of NMR spin lattice relaxation for spin-1. *J. Magn. Res. A.* 103:1–7.

Morrison, C., and M. Bloom. 1994. Orientation dependence of H-2 nuclear magnetic resonance spin-lattice relaxation in phospholipid and phospholipid-cholesterol systems *J. Chem. Phys.* 101:749–763.

Mulliken, R. S. 1955. Electronic population analysis on LCAO-MO molecular wave functions. *Int. J. Chem. Phys.* 23:1833.

Nagle, J. F. 1993. Area/lipid of bilayers from NMR. *Biophys. J.* 64: 1476–1481.

Nagle, J. F., and M. C. Wiener. 1988. Structure of fully hydrated bilayer dispersions. *Biochim. Biophys. Acta.* 942:1–10.

Oldfield, E., M. Meadows, D. Rice, and R. Jacobs. 1978. Spectroscopic studies of specifically labelled membrane systems: nuclear magnetic resonance investigation of the effects of cholesterol in model systems. *Biochemistry.* 17:2727–2740.

Pickar, A. D., and R. Benz. 1978. Transport of oppositely charged lipophilic probe ions in lipid bilayer membranes having various structures. *J. Membr. Biol.* 44:353–376.

Portlock, S. H., Y. Lee, J. Tomich, and L. K. Tamm. 1992. Insertion and folding of the N-terminal amphiphilic signal sequence of the mannitol and glucitol permeases of Escherichia coli. *J. Biol. Chem.* 267: 11017–11022.

Rice, D., and E. Oldfield. 1979. Deuterium nuclear magnetic resonance studies of the interaction between dimyristoylphosphatidylcholine and gramicidin A′. *Biochemistry.* 18:3272–3279.

Robinson, A. J., W. G. Richards, P. J. Thomas, and M. M. Hann. 1994. Head group and chain behavior in biological membranes: a molecular dynamics computer simulation. *Biophys. J.* 67:2345–2354.

Ryckaert, J. P., and A. Bellemans. 1975. Molecular dynamics of liquid *n*-butane near its boiling point. *Chem. Phys. Lett.* 30:123–125.

Ryckaert, J. P., and A. Bellemans. 1978. Molecular dynamics of liquid alkanes. *Far. Disc. Chem. Soc.* 66:95–106

Sanders, C. R. 1993. Solid state ^{13}C NMR of unlabeled phosphatidylcholine bilayers: spectral assignments and measurement of carbon-phosphorus dipolar couplings and ^{13}C chemical shift anisotropies. *Biophys. J.* 64:171–181.

Seelig, A. 1987. Local anesthetics and pressure: a comparison of dibucaine binding to lipid monolayers and bilayers. *Biochim. Biophys. Acta.* 899: 196–204.

Seelig, J., and A. Seelig. 1980. Lipid conformation in model membranes and biological membranes. *Q. Rev. Biophys.* 13:19–61.

Simon, S. A., and T. J. McIntosh. 1989. Magnitude of the solvation pressure depends on dipole potential. *Proc. Natl. Acad. Sci. USA.* 86: 9263–9267.

Snyder, R. G. 1967. Vibrational study of the chain conformation of the liquid *n*-paraffins and molten polyethylene. *J. Chem. Phys.* 47: 1316–1360.

Sudhakar, P. V., C. Singh, E. Jakobsson, and S. Subramaniam. 1995. Molecular dynamics simulations on cation channel models. *Biophys. J.* 68:A371.

van Gunsteren, W. F., and H. J. C. Berendsen. 1987. Groningen Molecular Simulation (GROMOS) Library Manual. Biomos, Groningen, The Netherlands.

Venable, R. M., Y. Zhang, B. J. Hardy, and R. W. Pastor. 1993. Molecular dynamics simulations of a lipid bilayer and of hexadecane: an investigation of membrane fluidity. *Science.* 262:223–226.

von Heijne, G. 1994. Membrane proteins: from sequence to structure. *Annu. Rev. Biophys. Biomol. Struct.* 23:167–192.

White, S. H. 1980. Small phospholipid vesicles: internal pressure, surface tension, and surface free energy. *Proc. Natl. Acad. Sci. USA.* 77: 4048–4050.

Wiener, M. C., and S. H. White. 1992a. Structure of a fluid dioleoylphosphatidylcholine bilayer determined by joint refinement of x-ray and neutron diffraction data. II. Distribution and packing of terminal methyl groups. *Biophys. J.* 61:428–433.

Wiener, M. C., and S. H. White. 1992b. Structure of a fluid dioleoylphosphatidylcholine bilayer determined by joint refinement of x-ray and neutron diffraction data. III. Complete structure. *Biophys. J.* 61: 434–447.

Zheng, C., and G. Vanderkooi. 1992. Molecular origin of the internal dipole potential in lipid bilayers: calculation of the electrostatic potential. *Biophys. J.* 63:935–941.

Zhou, F, and K. Schulten. 1995. Molecular dynamics study of a membrane-water interface. *J. Phys. Chem.* 99:2194–2208.